# Molecularly Imprinted Polymer Grafted Porous Au-Paper Electrode for an Microfluidic Electro-Analytical Origami Device

*Lei Ge, Shoumei Wang, Jinghua Yu,* Nianqiang Li, Shenguang Ge, and Mei Yan*

**Molecular imprinting technique is introduced into microfluidic paper-based analytical devices (μ-PADs) through electropolymerization of molecular imprinted polymer (MIP) in a novel Au nanoparticle (AuNP) modified paper working electrode (Au-PWE). This is fabricated through the growth of a AuNP layer on the surfaces of cellulose fibers in the PWE. Due to the porous morphology of paper as well as the high specific surface area and conductivity of the resulting AuNP layer on the cellulose fibers, the effective surface area and the sensitivity of the Au-PWE is enhanced remarkably. Based on this novel MIP-Au-PWE and the principle of origami, a microfluidic MIP-based electro-analytical origami device (μ-MEOD), comprised of one auxiliary pad surrounded by four sample tabs, is developed for the detection of D-glutamic acid in a linear range from 1.2 nM to 125.0 nM with a low detection limit of 0.2 nM. The selectivity, reproducibility, and stability of this μ-MEOD are investigated. This μ-MEOD would provide a new platform for high-throughput, sensitive, specific, and multiplex assay as well as point-of-care diagnosis in public health, environmental monitoring, and the developing world.**

## 1. Introduction

The last five years have witnessed fast progress in the field of microfluidic paper-based analytical devices (μ-PADs),[1,2] which represent new and outstanding approaches to simple, portable, disposable, and inexpensive devices for molecular analysis and monitoring health. Paper is a porous cellulose fiber web with large surface area, and the porous nature not only fulfills the primary tasks such as diagnostic tests using body fluids and fluid transport, but also makes it possible to pattern hydrophilic channels separated by hydrophobic walls of photoresist/polymer,[3–7] inks,[8,9] wax,[10–12] or by plasma treatment,[13] laser treatment[14] and cutting method.[15] In addition, these μ-PADs can be well applied not only in point-of-care testing but also in field analysis in remote locations with limited facilities.[16] Inspired by this simple technique, many groups have paid great efforts to the development of μ-PADs, including fabrication methods for μ-PADs,[17–19] functionalizations for μ-PADs,[20–25] and analytical methods[26–31] on μ-PADs. The success of μ-PADs arises from three main factors: low cost, ease of operation, and ability to function without any external pumps. We have also proposed several analytical methods on μ-PADs for the detection of small molecules[28] and proteins.[32–35]

However, although the current paper-based analytical methods on μ-PADs showed remarkable sensitivity and selectivity, many of them reported to date have relied almost exclusively on the use of sophisticated biological receptors, such as enzymes,[28,36] antibodies,[26,37,38] or DNA,[39–41] as biochemical recognition elements. Due to their biological derivation, these bio-molecules may suffer from limitations when used in diagnostic applications, for example, denaturation, possible instability during manufacture and transportation. Molecular imprinting technique is a well-known and widely used tool to produce synthetic bio-mimetic receptors for target molecules.[42] The target molecule, or a derivative thereof, acts as a template around which interacting and cross-linking monomers are arranged and polymerized to form a cast-like shell. After removal of the template, binding cavities that are complementary in shape, size, and position of chemical functionalities with respect to the template appear, and the resulting material can specifically recognize and bind its target. In comparison with natural bio-recognition materials like antibodies, molecularly imprinted polymers (MIPs) offer advantages like superior physical and chemical stability, specific recognition, ease of mass preparation, and easy availability and thus have found applications in wide areas including separation, sensors, and catalysis.[43]

For practical clinical application, now tremendous efforts have been focused on developing low-cost and portable methods. Electrochemical methods,[44] which distinguish themselves by convenient miniaturization and integration, easy

Dr. L. Ge, Prof. J. Yu, Dr S. Ge, Prof. M. Yan
School of Chemistry and Chemical Engineering
University of Jinan
Jinan 250022, China
E-mail: ujn.yujh@gmail.com
Dr. S. Wang
Shandong Provincial Key Laboratory of Preparation and Measurement of Building Materials
University of Jinan
250022, Jinan, China.
Dr. N. Li
School of Information Science and engineering
University of Jinan
250022, Jinan, China.

**DOI: 10.1002/adfm.201202785**

signal quantification, simple instrumentation, and low cost of the entire assay, can be ideal alternatives. In addition, electrochemical methods have, in recent years, received the major share of the attention in development of analytical methods for μ-PADs.[45–47] In our group, we have tried to improve the specificity of electrochemical method on lab-on-paper devices through development of electrochemical immunoassay on μ-PADs for the sensitive and specificity diagnosis of cancer markers (multianalyte immunoassay) at nanogram per milliliter concentrations using novel μ-PADs for signal transduction and acquisition.[33,48] Therefore, in this work, a novel microfluidic electro-analytical origami device (μ-EOD) (**Scheme 1**) was designed to demonstrate the development of molecular imprinting technique on μ-PADs. As shown in Scheme 1, this μ-EOD, comprised of one auxiliary pad surrounded by four sample tabs, was fabricated through wax-printing. After folding at the predefined fold line, the wax patterns around the screen-printed electrodes on sample tab and auxiliary pad constituted reservoir of the paper electrochemical cell. In addition, as shown in Scheme 1A,B, the screen-printed carbon working electrode on the sample tab together with the paper sample zone was denoted as "paper working electrode (PWE)" below (**Scheme 2**A).

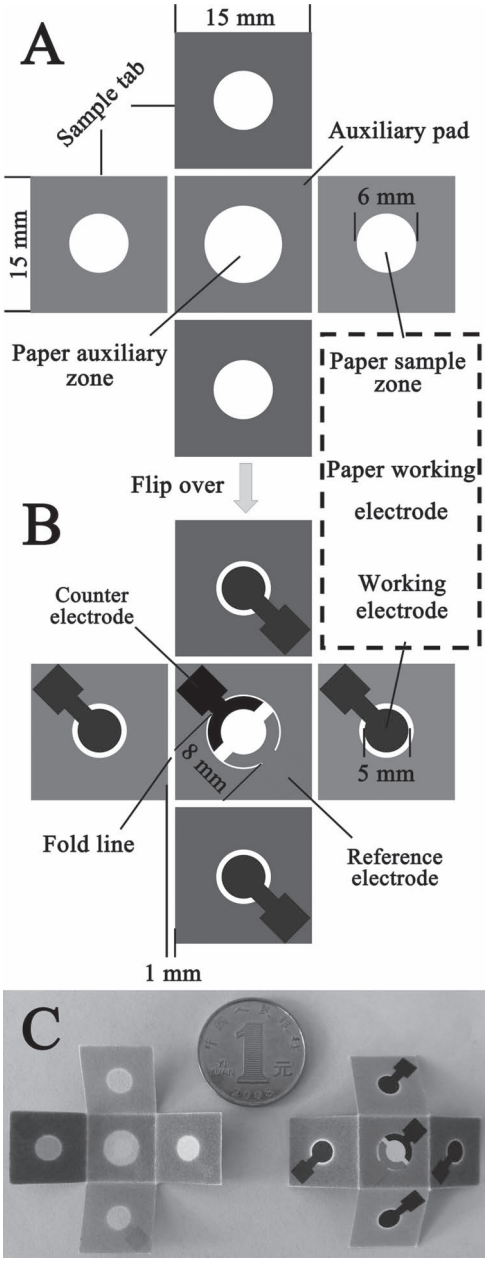


**Scheme 1.** The schematic representation, size, and shape of this μ-EOD. A) One side of the μ-EOD without the screen-printed electrodes; B) The reverse side of (A) with the screen-printed electrodes; C) Picture of this μ-EOD.

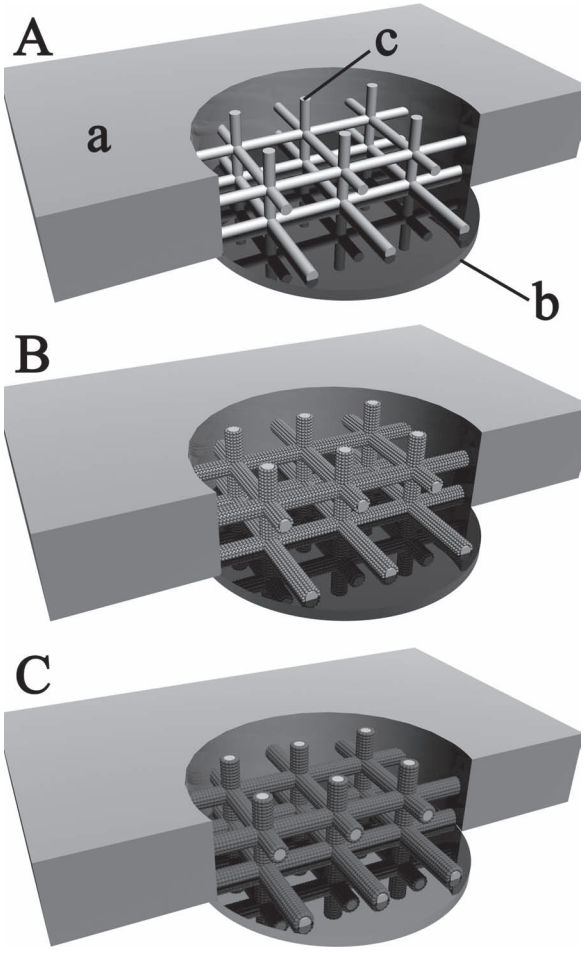


**Scheme 2.** Schematic representation of the fabrication procedures for this μ-MEOD. A) bare PWE: (a) wax-penetrated paper, (b) screen-printed carbon working electrode, (c) unprinted porous paper as paper sample zone; B) Growth of a AuNP layer on the surfaces of cellulose fibers in bare PWE; C) Electropolymerization of the MIP layer on the surfaces of AuNP coated cellulose fibers in Au-PWE.

Briefly, in this work, an Au nanoparticle (AuNP) layer was grown on the surfaces of cellulose fibers from AuNP seeds in the paper sample zone of PWE to fabricate novel porous Au-PWE on this μ-EOD. Due to the high ratio of surface area to weight (9.5 $m^2/g$)[49] and porous structure of paper as well as the high conductivity of Au, the active surface area and the sensitivity of this Au-PWE was much higher than that of a bare one (unmodified PWE). Finally, a microfluidic MIP-based electro-analytical origami device (μ-MEOD) was fabricated through

grafting a layer of MIP in this porous Au-PWE by electropolymerization. Glutamic acid is a main excitatory neurotransmitter in the brain,[50] and increase of extra-cellular glutamic acid is believed to be partially responsible for brain damage resulting from the central nervous and mental disorders.[51] Therefore, D-glutamic acid was used as a model analyte to illustrate the feasibility of this $\mu$-MEOD.

## 2. Results and Discussion

In this work, molecular imprinting technique was introduced into the $\mu$-EOD through the electropolymerization of poly-o-phenylenediamine (Po-PD) MIP in the paper sample zone of PWE on sample tab (Scheme 2C) using cyclic voltammetry (CV) in the presence of D-glutamic acid, which was used as a model template. Prior to the electropolymerization, growth of a AuNP layer from AuNP seeds on the surfaces of cellulose fibers in the paper sample zone of PWE was implemented to fabricate porous Au-PWE (Scheme 2B) with enhanced conductive and enlarged effective surface area for the further grafting of MIP.

### 2.1. Characterization of Au-PWE

The transmission electron microscopy (TEM) image (**Figure 1**A) of the as-prepared AuNP seeds solution revealed a highly monodispersed AuNP seeds suspension with an average diameter of ~3.5 nm. As shown in Figure 1B, the porous bare paper sample zone, possessed high ratio of surface area to weight (9.5 $m^2/g$)[49] with rough cellulose fibers, could offer an excellent adsorption microenvironment for the AuNP seeds. It can be seen that there was no apparent structural and surface difference between the bare (Figure 1B) and the AuNP seeded (Figure 1C) cellulose fibers in the paper sample zone of PWE due to the small particle size of AuNP seeds (Figure 1D). In addition, the successful immobilization of AuNP seeds on cellulose fibers was confirmed by X-ray photoelectron spectroscopy (XPS) and the peaks observed at 82.6 and 86.4 eV were ascribed to metallic gold (**Figure 2**A). The growth process of the AuNP layer on the surfaces of cellulose fibers was tracked by scanning electron microscopy (SEM) characterization (**Figure 3**). As the growth time increased (from 0 to 5 min), the AuNP seeds were rapidly enlarged by incubating in the growth solution under the self-catalytic reduction mechanism of AuNP growth[52] (Figure 3A,C,E). Finally, as shown in Figure 3B,D,F, a continuous and dense AuNP conducting layer with interconnected AuNPs on the cellulose fiber surface in paper sample zone was observed, indicated that a good coverage of AuNPs on the surfaces of the cellulose fibers was obtained after 10 min of growth. Therefore, the conductivity of the paper sample zone with AuNP modification ($1.15 \times 10^{-5}$ $\Omega \cdot$cm, measurement details in Supporting Information) was enhanced remarkably compared to that without AuNP modification (insulating (open loop)) under the same condition in each case. In addition, as shown in Figure 3B, the AuNP modified paper sample zone still maintained good porous structure after the growth process, which would benefit the further MIP modification and analytical application.

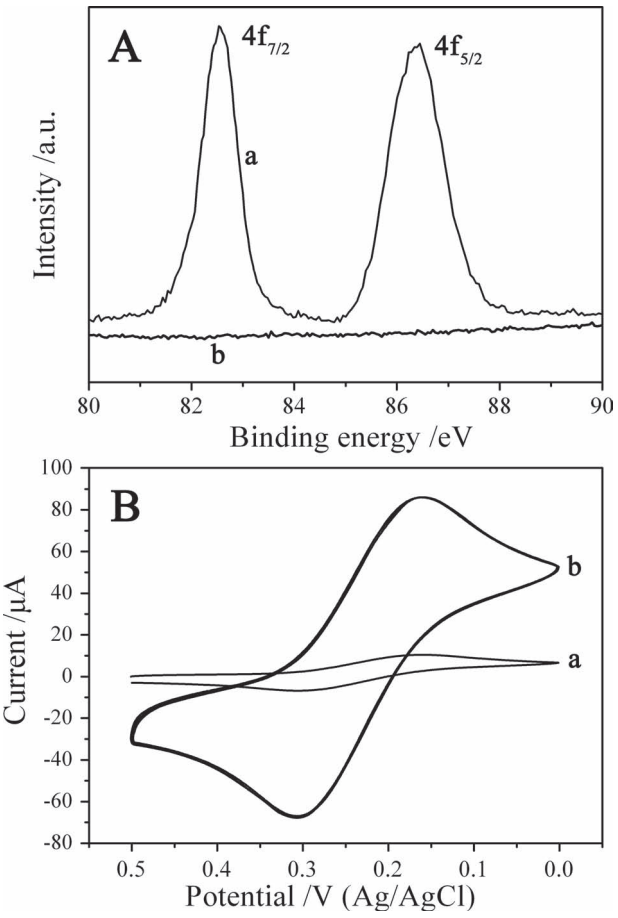


**Figure 2.** A) XPS of (a) the AuNP seeded paper sample zone of PWE and (b) bare paper sample zone of PWE; B) CVs of (a) bare PWE and (b) porous Au-PWE under 20 successive scans. Scan rate: 50 $mV \cdot s^{-1}$.

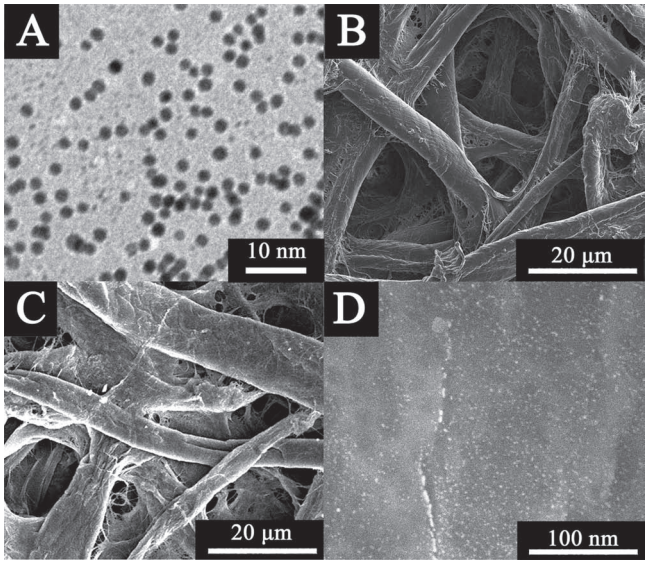


**Figure 1.** A) TEM image of the as-prepared AuNP seeds solution; SEM images of B) bare paper sample zone of PWE, C) AuNP seeded paper sample zone of PWE; D) SEM image of AuNP seeds on the surface of the cellulose fiber.

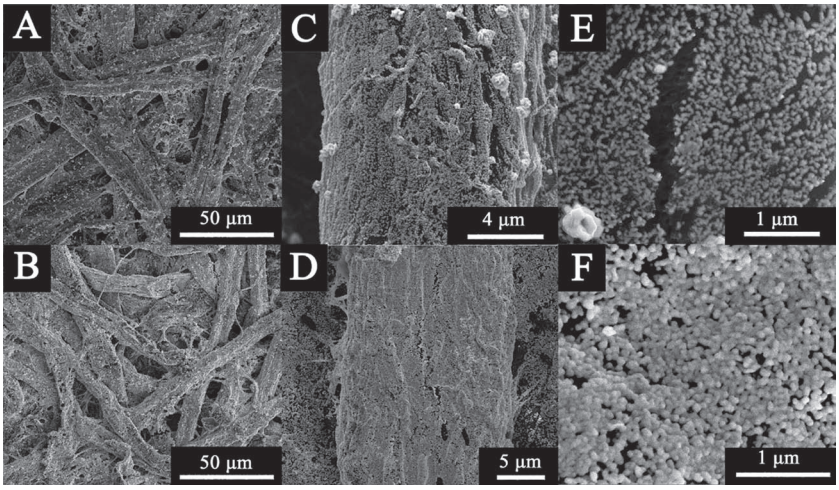


**Figure 3.** Enlarged AuNPs on the surfaces of cellulose fibers in paper sample zone of PWE at different growth time under different magnification: A,C,E) After 5 min of growth; B,D,F) after 10 min of growth.

The electrochemical properties of the resulted porous Au-PWE were investigated through CV toward 10.0 mM $[Fe(CN)_6]^{3-/4-}$ solution containing 0.5 M KCl (Figure 2B). The bare PWE was also characterized under the same conditions for comparison. As shown in Figure 2B, the bare PWE exhibited one set of well defined redox peaks toward $[Fe(CN)_6]^{3-/4-}$ (Curve a). For the Au-PWE, there was a sharp increase of the peak current (Curve b). The CV curves showed that the Au-PWE had a significant higher peak current and larger CV area compared with the bare one, indicating that the porous Au-PWE had a much larger effective surface area, which may be attributed to the high effective surface area of the AuNP layer on cellulose fibers and the porous morphology of paper. The Au-PWE was scanned successfully for 20 cycles toward $[Fe(CN)_6]^{3-/4-}$ solution and no observable peak current and position change was found (Curve b in Figure 2B).

### 2.2. Characterization of Electro-Polymerized MIP/NIP in Au-PWE

Electropolymerization of Po-PD for the synthesis of MIP layer was carried out by CV scanning toward acetate buffer solution containing template (D-glutamic acid) and monomer (o-PD) in Au-PWE at room temperature. As shown in **Figure 4**, the distinct and irreversible anodic peaks, obtained in the first scan at ≈+0.7 V corresponding to the oxidation of o-PD, decreased considerably with increasing numbers of consecutive scan cycles, indicated that the polymers created an insulating layer (**Figure 5** and Scheme 2C) on the surfaces of AuNP layer and covered the AuNP layer to restraint the further oxidation of the o-PD. Similarly, the non-imprinted polymer (NIP) grafted Au-PWE was also prepared under the same experimental conditions in each case without adding D-glutamic acid to the polymerization solution. In addition, as shown in Figure 4, there was no remarkable difference between the CVs related to the electropolymerization of NIP without adding the template (Figure 4A) and the CVs related to the electropolymerization of MIP in the presence of the template (Figure 4B). It can be deduced that the presence of the electro-inactive D-glutamic acid in the paper electrochemical cell was not electrochemically altered while the Po-PD was growing around it.

The CVs of the MIP-Au-PWE were recorded toward a 10.0 mM $[Fe(CN)_6]^{3-/4-}$ solution containing 0.5 M KCl. **Figure 6**A showed the relation between the peak current and the surface condition of the cellulose fibers in the MIP-Au-PWE. Due to the resulted insulating MIP layer which covered the surfaces of the AuNP layer, the oxidation-reduction peaks changed from curve-a to curve-b accompanied by a remarkable decrease in the peak current and an increase in the peak-to-peak separation between the cathodic and anodic waves. This fact demonstrated that the electron transfer kinetics of $[Fe(CN)_6]^{3-/4-}$ was obstructed. However, the oxidation-reduction currents were still observable in the CV (curve-b) probably due to the pinholes or defects in the MIP layer.[53] Thus, in order to lower the leakage of the MIP layer and cover the surfaces of Au-PWE as completely as possible to leave only biding cavities, a long chain 1-dodecanethiol was employed to fill the pinholes or defects in the MIP layer (Curve c). After the template was removed, an obvious oxidation-reduction peak was observed again (Curve d), indicated

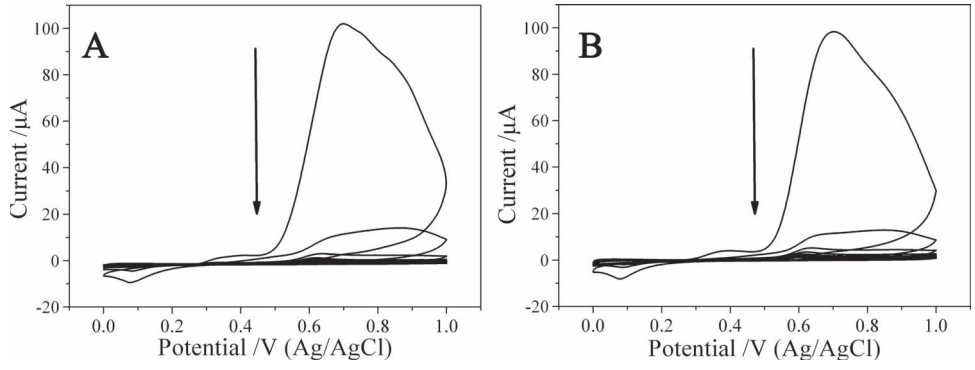


**Figure 4.** CVs for electropolymerization of 10 μM o-PD A) without or B) with 6 μM D-glutamic acid in Au-PWE in a potential range between 0 V and 1.0 V. Scan rate: 50 mV·s$^{-1}$.

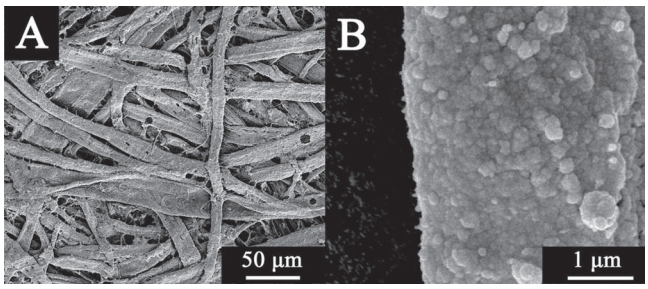


**Figure 5.** SEM images of the electro-polymerized MIP on the AuNP coated cellulose fibers in the paper sample zone of Au-PWE under different magnification.

that the more available access for $[Fe(CN)_6]^{3-/4-}$ through the MIP layer. It can be ascribed that after the removal of template, the electronic transmission of $[Fe(CN)_6]^{3-/4-}$ through the resulted binding cavities to the surfaces of the AuNP layer became more easily. The decrease in the peak current from Curve d and Curve e was attributed to the obstruction of access to $[Fe(CN)_6]^{3-/4-}$ through the MIP layer after D-glutamic acid rebinding. This may be explained by the molecular recognition between D-glutamic acid and the binding cavities in MIP layer, which blocked the electron transfer of the $[Fe(CN)_6]^{3-/4-}$ redox reaction to the Au-PWE. These results confirmed that the template has been embedded in the MIP.

In contrast, for the NIP-Au-PWE (Figure 6B), the oxidation-reduction current decreased dramatically from Curve a to Curve b due to that an insulating NIP layer was electro-polymerized and covered the surfaces of the AuNP layer. The change in oxidation-reduction current was negligible (Curves b–d) after the template removal step because no cavities with binding sites were obtained in the absence of D-glutamic acid. This indicated that the NIP-Au-PWE was non-selective and failed to recognize D-glutamic acid.

Electrochemical impedance spectroscopy (EIS) of the resulting MIP-Au-PWE could also give detail information about the modification process. EIS was carried out in a background solution of 5 mM $[Fe(CN)_6]^{3-/4-}$ at a bias potential of 170 mV (vs Ag/AgCl). The frequency range was 100 MHz to 10 KHz. In EIS, the diameter of the semicircle at higher frequencies corresponds to the electron-transfer resistance ($R_{et}$); a change in the value of $R_{et}$ was associated with the blocking behavior of the modification processes in the PWE, and was reflected in the EIS as a change in the diameter of the semicircle at high frequencies. Herein, the electron-transfer of $[Fe(CN)_6]^{3-/4-}$ onto the surfaces of Au-PWE was blocked by the formation of MIP layer, which resulted in an increase in $R_{et}$. **Figure 7** showed the EIS (presented in the form of the Nyquist plot) of different surface conditions of the cellulose fibers in the PWE. The EIS of bare PWE revealed a relatively small semicircle domain (Curve a). After the growth of an AuNP layer, the EIS exhibited an obvious decrease in $R_{et}$ (Curve b). Remarkable increase in the $R_{et}$ value was observed after the electropolymerization of an insulating MIP (Curve c) layer on the surfaces of AuNP coated cellulose fibers in the Au-PWE, indicating that the compact MIP layer with low conductivity acted as a definite kinetic barrier for the charge transfer. After being treated with 1-dodecanethiol, the electron-transfer kinetics of the redox probe was slow down further (Curve d). The decrease of $R_{et}$ from Curve d to Curve e

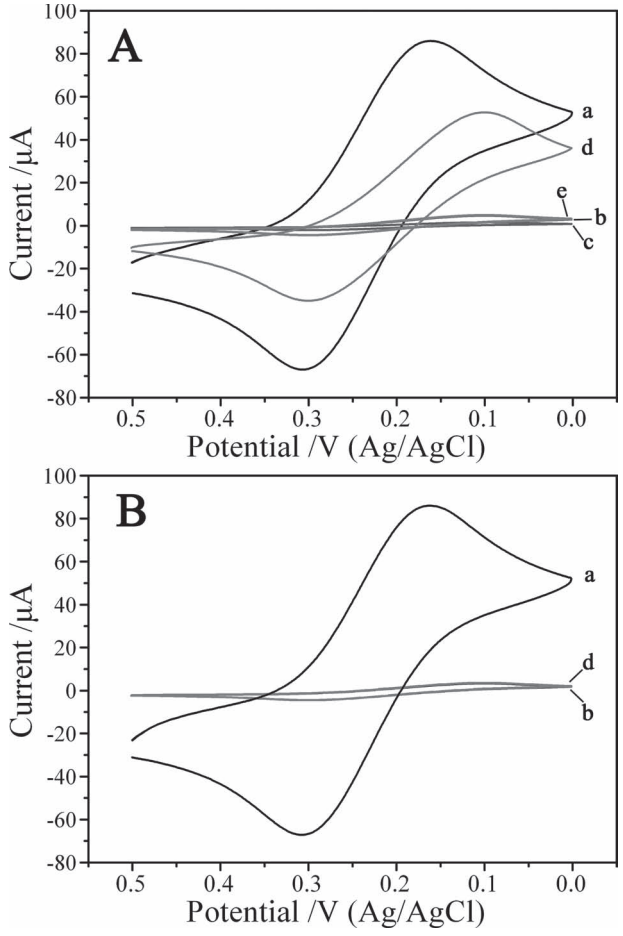


**Figure 6.** CVs of the A) MIP- and B) NIP-Au-PWE with different surface condition of the cellulose fibers: (a) Au-PWE; (b) MIP/NIP-Au-PWE; (c) MIP-Au-PWE treated with 1-dodecanethiol; (d) MIP/NIP-Au-PWE after template removal; (e) MIP-Au-PWE after rebinding.

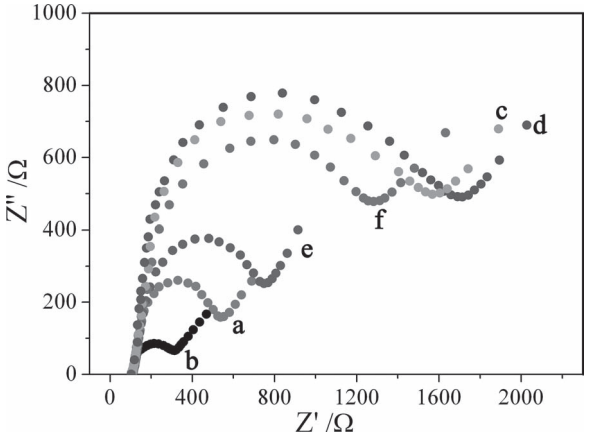


**Figure 7.** EIS of the PWE with different surface condition in 10.0 mM $[Fe(CN)_6]^{3-/4-}$ solution containing 0.5 M KCl: (a) bare PWE; (b) Au-PWE; (c) MIP-Au-PWE; (d) MIP-Au-PWE treated with 1-dodecanethiol; (e) MIP-Au-PWE after template removal; (f) MIP-Au-PWE after rebinding.

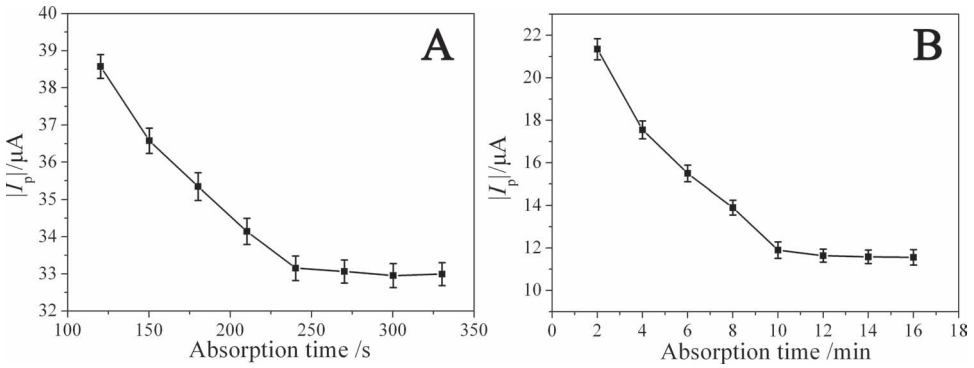


**Figure 8.** Effects of absorption time in A) MIP-Au-PWE and B) on MIP modified traditional flat Au electrode at 50 nM D-glutamic acid concentration.

could be attributed to the removal of template (D-glutamic acid) from the MIP layer and thus the unoccupied binding cavities in the MIP layer were available for the hexacyanoferrate redox probe to diffuse through. The increased $R_{et}$ from curve-e to ´Curve f signified that D-glutamic acid was rebounded to the MIP layer. This verified that the MIP layer had good capability to distinguish the target molecule. These results were accordant with CV assays as described in detail above. In addition, obvious hysteresis was observed in Figure 7 during the rebinding process, indicated that the as-prepared $\mu$-MEOD was not suitable for regeneration in its present form.

### 2.3. Choice of Absorption Time

The absorption time is an important parameter for the improvement of assay efficiency on μ-MEOD, which is usually controlled by the mass transport of template molecular and the kinetics of the rebinding on MIP layer. A fast assay is highly desired for lab-on-paper device in the field application. In this work, the absorption process was performed on-line at room temperature. As shown in **Figure 8**A, the electrochemical signals for 50.0 nM D-glutamic acid decreased quickly with the increasing of absorption time and then leveled off, indicated the equilibrium rebinding between the MIP and template. Hence, considering the optimal analytical performance and development of this method to high sample throughput, the absorption time of 240 s was selected in the further study. The absorption process in this MIP-Au-PWE needed shorter time compared with 10 min at room temperature on traditional MIP modified flat Au working electrode (Figure 8B). This is mainly due to the high surface-to-weight ratio, incompact porous structure and the small volume of the MIP-Au-PWE (0.18-mm thickness and 6-mm diameter). Thus, the template molecule should diffuse only short transport distances to reach the binding cavities.[26]

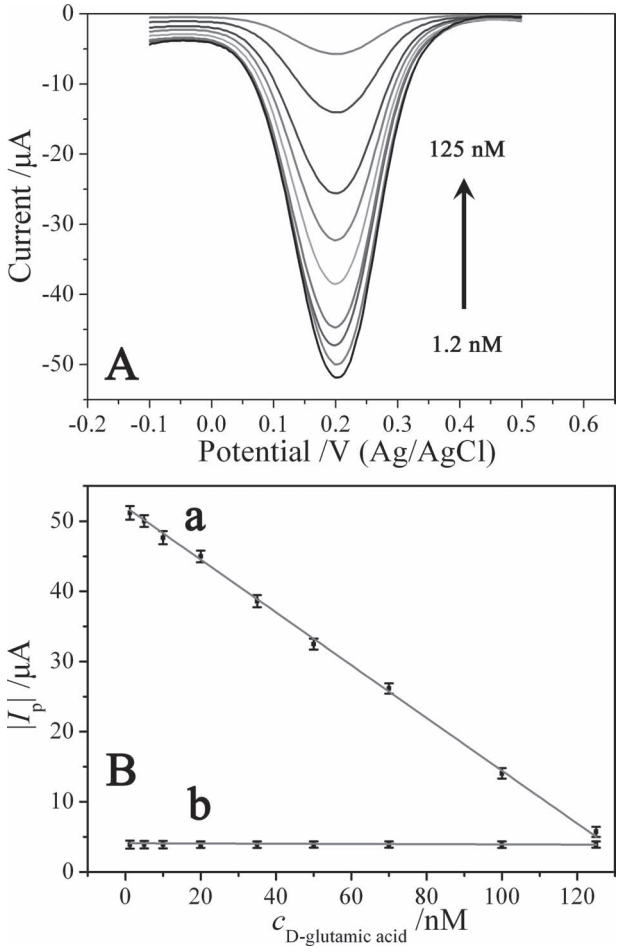


**Figure 9.** A) DPV responses for D-glutamic acid of this $\mu$-MEOD; B) Calibration curves for D-glutamic acid in (a) MIP-Au-PWE and (b) NIP-Au-PWE.

### 2.4. Analytical Performance

The analytical performance of this μ-MEOD was verified through the detection of D-glutamic acid in standard solution at various concentrations. **Figure 9**A showed the differential pulse voltammetry (DPV) response of this μ-MEOD from the oxidation peak current ($|I_p|$) of hexacyanoferrate after the absorption of D-glutamic acid. As seen in Figure 9A, with the increasing concentration of D-glutamic acid, the $|I_p|$ toward $[Fe(CN)_6]^{3-/4-}$ solution decreased over a wide concentration range of 1.2–125.0 nM. The plot of the $|I_p|$ decrease versus D-glutamic acid concentration was shown in Figure 9B (Curve a). The linear regression

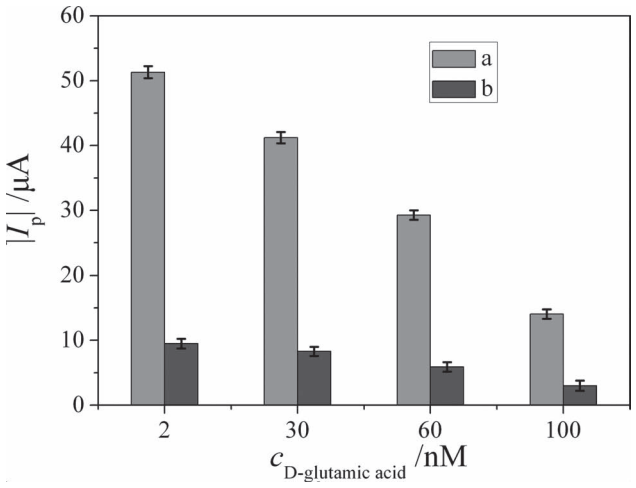


**Figure 10.** Comparison of the sensitivity between MIP-Au-PWE (a) and MIP-PWE (b) at different concentrations of D-glutamic acid.

equation was $|I_p|$ ($\mu$A) = 52.06–0.38 [D-glutamic acid] (nM) with a correlation coefficient of 0.9973. The limit of detection at a signal-to-noise ratio of 3 for D-glutamic acid was 0.2 nM. In the NIP-Au-PWE prepared through the electropolymerization under the same experimental conditions without the addition of template molecule, no peak current change was observed (Figure 9B, Curve b). These results also indicated that the DPV responses in the MIP-Au-PWE were resulted from the entrapment of the template D-glutamic acid molecules into the binding cavities in the imprinted polymer. In a further control experiment, MIP was electro-polymerized in the bare PWE under the same experimental conditions in each case. Compared with the MIP-Au-PWE (**Figure 10**a), the $|I_p|$ of the MIP-PWE that lacked the AuNP layer decreased tardily with the increasing of D-glutamic acid concentration and the $|I_p|$ intensities were low (Figure 10b), indicated that the sensitivity of this $\mu$-MEOD could be enhanced obviously through the AuNP modification in PWE.

The analytical reliability and application potential of this $\mu$-MEOD was evaluated by assaying four spiked clinical serum samples using the proposed method as well as the reference values obtained by high performance liquid chromatography (HPLC). If the levels of D-glutamic acid were over the calibration ranges, serum samples could be appropriately diluted with water prior to assay. The results gave the relative errors less than 5.0%, showing an acceptable agreement between the two methods (**Table 1**). Hence, the developed $\mu$-MEOD provided a possible application for the detection of D-glutamic acid in clinical diagnosis.

### 2.5. Specificity, Reproducibility, and Stability of This $\mu$-MEOD

To verify the specificity of the $\mu$-EOD modified with MIP for D-glutamic acid, experiments were performed by using some structurally related interferences in human serum, such as L-glutamic acid, D-tyrosine, D-phenylalanine, D-glutamine, D-aspartic acid, D-serine, D-cysteine, D-leucine, D-lysine, and ascorbic acid. The structures of the compounds tested and corresponding DPV peak current under different concentrations of the interferences were shown in Supporting Information Table S1. Almost no interference (<3.0%) was observed with other amino acids and ascorbic acid, even at a high concentration of 1.0 μM. It is notable that L-glutamine showed apparent DPV peak current decrease due to its analogous structure, which could be easily embedded into the binding cavities accessible for D-glutamic acid. This indicated that the binding cavities that can recognize the D-glutamic acid, created through electropolymerization method, were based on the shape selection and orientation of functional groups. These results confirmed that the $\mu$-MEOD based on the artificial D-glutamic acid receptor had a good selectivity for its recognition. As seen from Supporting Information Table S1, the $\mu$-MEOD with D-glutamic acid imprinted polymer showed very weak current response to L-glutamic acid, indicated that the enantioselectivity of this $\mu$-MEOD toward the template molecules was also very excellent.

**Table 1.** Assay results of real human serum by the proposed and reference method.

| Sample | D-glutamic acid concentration [nM] | |
|---|---|---|
| | Proposed $\mu$-MEOD found[a] ±S.D.[b] | Reference HPLC method found[a] ±S.D.[b] |
| Sample-1 | 4.49 ± 0.16 | 4.66 ± 0.13 |
| Sample-2 | 13.15 ± 0.27 | 13.98 ± 0.22 |
| Sample-3 | 57.54 ± 0.33 | 56.51 ± 0.25 |
| Sample-4 | 92.73 ± 0.56 | 94.36 ± 0.29 |

[a]Average of eleven measurements; [b]Standard deviation.

The reproducibility of this $\mu$-MEOD for D-glutamic acid was investigated with inter-assay precision. The relative standard deviation for the parallel detection of 0, 10.0, and 50.0 nM D-glutamic acid with ten $\mu$-MEODs was 2.05%, 2.11%, and 1.93%, respectively. When the $\mu$-MEODs were stored and measured at intervals of three days, no obvious change was observed after 10 weeks under ambient conditions. These results indicated that this $\mu$-MEOD had better reproducibility, stability, and precision during manufacture, storage or long-distance transport to remote regions and developing countries compared with previous antibody-based paper immunodevice.[33,48]

## 3. Conclusion

In this work, a novel lab-on-paper device, combining the high-throughput and sensitivity of this $\mu$-EOD and the low-cost, stability, and selectivity of molecular imprinting technique, is developed here. The molecularly imprinted polymer of Po-PD is successfully grafted in a novel porous Au-PWE as recognition element through the simple, convenient, and low-cost electropolymerization method for chiral and sensitive discrimination of D-glutamic acid. It is the first molecularly imprinted material prepared directly on $\mu$-PADs. This $\mu$-MEOD with short absorption time, acceptable sensitivity, low detection limit, wide

linear concentration range, good stability and reproducibility is also the first MIP-based lab-on-paper device for point-of-care testing. In addition, the proposed MIP-Au-PWE on μ-MEOD could not only be imprinted as artificial receptors for enantioselective recognition of other amino acids, drugs, and proteins, but also be readily integrated with other signal reporting mechanism on μ-PADs such as electrochemiluminescence and photoelectrochemistry.

## 4. Experimental Section

*Reagents and Materials*: All reagents were of analytical-reagent grade and directly used for the following experiments as supplied. Ultrapure water obtained from a Millipore water purification system (>18.2 MΩ, Milli-Q, Millipore) was used in all assays and solutions. L-glutamic acid, D-glutamic acid, L-glutamine, D-cysteine, D-leucine, D-serine, D-lysine, D-tyrosine, D-phenylalaine, D-aspartic acid, o-phenylenediamine (o-PD), and 1-dodecanethiol were purchased from Sigma-Aldrich. Tetrachloroauric acid ($HAuCl_4$) as the precursor for the formation of AuNP seeds was purchased from Shanghai Sangon Biological Engineering Technology & Services Co. Potassium ferricyanide, $NaBH_4$, and sodium citrate were products from Shanghai Chemical Reagent Co. Whatman chromatography paper #1 (58.0 cm × 68.0 cm) was obtained from GE Healthcare Worldwide (Pudong Shanghai, China) and used with further adjustment of size (A4 size).

*Preparation of the μ-EOD*: The preparation of this μ-EOD was similarly to our previous work[54] with large modifications and a detailed procedure was described below. Wax was used as the paper hydrophobization and insulation agent in this work to construct hydrophobic barrier on paper. As shown in Scheme 1A, this origami device was comprised of an auxiliary pad surrounded by four sample tabs with the same size (15.0 mm × 15.0 mm). The shape of hydrophobic barrier on origami device, which contained a paper auxiliary zone (8 mm in diameter) on auxiliary pad and four paper sample zones (6 mm in diameter) on four sample tabs respectively, was designed using Adobe illustrator CS4. The entire origami device could be produced in bulk on an A4 paper sheet by a commercially available solid-wax printer (Xerox Phaser 8560N color printer) (Supporting Information Figure S1). Owing to the porous structure of paper, the melted wax can penetrate into the paper network to decrease the hydrophilicity of paper remarkably (Supporting Information Figure S2). After the curing process, the unprinted area (paper auxiliary zone and paper sample zones) still maintained good hydrophilicity, flexibility, and porous structure and will not affect the further screen-printing of electrodes and modifications.[12,55]

Between the each tab and auxiliary pad, the unprinted line (1 mm in width) was defined as fold line, which could ensure that the paper sample zones on the four tabs were properly and exactly aligned to the paper auxiliary zone on auxiliary pad after folding, due to the difference of flexibility between the printed and unprinted area after baking.[34] The unprinted hydrophilic area (paper auxiliary zone and paper sample zones) constituted the reservoir of the paper electrochemical cell (~40 μL) after being folded at the predefined fold line. Then, the wax-penetrated paper sheet was ready for screen-printing of electrodes on their corresponding paper zones (Scheme 1B and Supporting Information Figure S3). The electrode array consisted of a screen-printed Ag/AgCl reference electrode and carbon counter electrode on the paper auxiliary zone and four screen-printed carbon working electrodes (5 mm in diameter) on the four paper sample zones respectively. After folding, the three screen-printed electrodes (working electrode, reference electrode, and counter electrode) will be connected once the paper electrochemical cell was filled with solution. Finally, the paper sheet was cut into individual origami device for further modifications (Scheme 1C).

*Preparation of the μ-MEOD*: As shown in Scheme 2, the μ-MEOD was fabricated through electropolymerization of Po-PD MIP in the paper sample zone of PWE on sample tabs (Scheme 2C) using CV in the presence of template. Prior to the electropolymerization, growth of AuNP layer on the surfaces of cellulose fibers in the paper sample zone of PWE was implemented to fabricate porous Au-PWE (Scheme 2B) with enhanced conductivity and enlarged effective surface area for the further grafting of MIP.

The suspension of AuNP seeds was prepared by using $NaBH_4$ as reductant and stabilized with sodium citrate according to the literature.[56] Then, as-prepared AuNP seeds solution (60.0 μL) was divided into four portions and dropped into the four bare PWEs (Scheme 2A), respectively. Then the origami device was equilibrated at room temperature for 1 h to optimize the surface immobilization of AuNP seeds on cellulose fibers. After rinsing with water thoroughly according to the method in our previous work[30] to remove loosely bound AuNP seeds, freshly prepared growth aqueous solution (15 μL) of phosphate buffer (0.01 M, pH 7.0) containing $HAuCl_4$ ($1.2 \times 10^{-3}$ M), cetyltrimethylammonium chloride ($2 \times 10^{-3}$ M), and $H_2O_2$ ($7.2 \times 10^{-3}$ M) for seeds growth was applied into the AuNP seeded PWEs, respectively, and incubated at room temperature for 10 min. During the growth process, the Au NP seeds acted as catalysts for the reduction of $AuCl_4^-$ by $H_2O_2$, resulting in the enlargement of the AuNP seeds.[52] Subsequently, the resulting Au-PWE was washed with water thoroughly. Thus a layer of interconnected AuNPs on cellulose fibers with good conductivity were obtained (Scheme 2B), which were dried at room temperature for 20 min.

The electropolymerization of MIP on AuNP coated cellulose fibers in the Au-PWEs on the four sample tabs were performed sequentially as below (Supporting Information Scheme S1A,B): First, the sample tab was folded down below the auxiliary pad and clamped with a home-made device-holder similar to our previous work,[54] which was comprised of two circuit boards (named Board-A and Board-B respectively below) with conductive pads on them, to fix and connect this origami device to the electrochemical workstation (Shanghai CH Instruments Co., China) as shown in Supporting Information Scheme S1A. Second, a acetate buffer solution (40 μL, 0.1 M, pH = 5.2, 25 °C) containing o-PD (10 μM) and D-glutamic acid (6 μM) were applied into the paper electrochemical cell through the hole on Board-B followed by twenty cycles of CVs in a potential range between 0 and 1.0 at a scan rate of 50 $mV \cdot s^{-1}$ at room temperature (Supporting Information Scheme S1B). Following the same procedures described above, the other three MIP-Au-PWEs could be also obtained. Finally, the paper auxiliary zone and the resulting MIP-Au-PWEs were washed thoroughly by the acetate buffer solution to remove the unreacted o-PD. After electropolymerization, the template molecules entrapped in and adsorbed on the MIP layer were removed by washing with 50 mM HCl and water alternately. As a result, the μ-MEOD with MIP layer that had stereo specific cavities for D-glutamic acid was obtained. The SEM images of this μ-MEOD were recorded on a JEOL JSM-5510 scanning electron microscope. TEM investigations were performed using JEOL 4000 EX microscope. EIS was performed on an IM6x electrochemical working station (Zahner Co., Germany). Similarly, the NIP grafted Au-PWE was also prepared under the same experimental conditions in each case without adding D-glutamic acid to the polymerization solution.

*Assay Procedure of this μ-MEOD*: The electrochemical assay procedures on this μ-MEOD were also shown in Supporting Information Scheme S1, and detailed procedures were described below. In this work, DPV was employed for the current measurements, which was relatively sensitive compared to the conventional CV method. To carry out the electrochemical detections, four spiked human serum samples (15.0 μL respectively) containing different concentration of D-glutamic acid was added into the four MIP-Au-PWEs, respectively, and allowed to absorbed for 240 s at room temperature to reach the equilibrium binding, followed by washing with water for preventing the nonspecific binding and achieving the best possible signal-to-background ratio. Thereafter, one sample tab was folded down below the auxiliary pad and clamped into the device-holder mentioned above to make the μ-MEOD stacked closely (Supporting Information Scheme S1A). Ultimately, KCl solution (40.0 μL, 0.5 M) containing $[Fe(CN)_6]^{3-/4-}$ (10.0 mM) was dropped into the paper electrochemical cell through the hole on Board-B (Supporting Information Scheme S1C) and then DPV measurements were performed

at room temperature in a potential range between –0.1 and 0.5 V, a modulation amplitude of 50 mV, a pulse width of 50 ms and a step potential of 5 mV. Similarly, the other three samples could be detected through repeating the same procedures mentioned above (Supporting Information Scheme S1A,C).

## Supporting Information

Supporting Information is available from the Wiley Online Library or from the author.

## Acknowledgements

This work was financially supported by Natural Science Research Foundation of China (21277058, 21175058, 21207048); Natural Science Foundation of Shandong Province, China (ZR2012BZ002) and Technology Development Plan of Shandong Province, China (2011GGB01153).

Received: September 25, 2012
Revised: December 11, 2012
Published online: January 18, 2013

[1] A. W. Martinez, S. T. Phillips, G. M. Whitesides, *Anal. Chem.* **2010**, *82*, 3.
[2] S. K. Sia, L. J. Kricka, *Lab Chip* **2008**, *8*, 1988.
[3] A. W. Martinez, S. T. Phillips, B. J. Wiley, M. Gupta, G. M. Whitesides, *Lab Chip* **2008**, *8*, 2146.
[4] J. Olkkonen, K. Lehtinen, T. Erho, *Anal. Chem.* **2010**, *82*, 10246.
[5] X. Li, J. Tian, W. Shen, *Cellulose* **2010**, *17*, 649.
[6] S. A. Klasner, A. K. Price, K. W. Hoeman, R. S. Wilson, K. J. Bell, C. T. Culbertson, *Anal. Bioanal. Chem.* **2010**, *397*, 1821.
[7] D. A. Bruzewicz, M. Reches, G. M. Whitesides, *Anal. Chem.* **2008**, *80*, 3387.
[8] X. Li, *Colloids Surf., B* **2010**, *76*, 564.
[9] K. Abe, K. Suzuki, D. Citterio, *Anal. Chem.* **2008**, *80*, 6928.
[10] Y. Lu, W. Shi, L. Jiang, J. Qin, B. Lin, *Electrophoresis* **2009**, *30*, 1497.
[11] Y. Lu, W. Shi, J. Qin, B. Lin, *Anal. Chem.* **2009**, *82*, 329.
[12] E. Carrilho, A. W. Martinez, G. M. Whitesides, *Anal. Chem.* **2009**, *81*, 7091.
[13] X. Li, J. Tian, T. Nguyen, W. Shen, *Anal. Chem.* **2008**, *80*, 9131.
[14] G. Chitnis, Z. Ding, C.-L. Chang, C. A. Savran, B. Ziaie, *Lab Chip* **2011**, *11*, 1161.
[15] E. M. Fenton, M. R. Mascarenas, G. P. López, S. S. Sibbett, *ACS Appl. Mater. Interfaces* **2009**, *1*, 124.
[16] A. W. Martinez, S. T. Phillips, M. J. Butte, G. M. Whitesides, *Angew. Chem. Int. Ed.* **2007**, *46*, 1318.
[17] A. W. Martinez, S. T. Phillips, G. M. Whitesides, *Proc. Natl. Acad. Sci. USA* **2008**, *105*, 19606.
[18] H. Liu, R. M. Crooks, *J. Am. Chem. Soc.* **2011**, *133*, 17564.
[19] E. Carrilho, S. T. Phillips, S. J. Vella, A. W. Martinez, G. M. Whitesides, *Anal. Chem.* **2009**, *81*, 5990.
[20] H. Hwang, S.-H. Kim, T.-H. Kim, J.-K. Park, Y.-K. Cho, *Lab Chip* **2011**, *11*, 3404.
[21] P. J. Bracher, M. Gupta, G. M. Whitesides, *J. Mater. Chem.* **2010**, *20*, 5117.
[22] X. Yang, O. Forouzan, T. P. Brown, S. S. Shevkoplyas, *Lab Chip* **2012**, *12*, 274.
[23] A. W. Martinez, S. T. Phillips, Z. Nie, C.-M. Cheng, E. Carrilho, B. J. Wiley, G. M. Whitesides, *Lab Chip* **2010**, *10*, 2499.
[24] A. V. Govindarajan, S. Ramachandran, G. D. Vigil, P. Yager, K. F. Bohringer, *Lab Chip* **2012**, *12*, 174.
[25] H. Chen, J. Cogswell, C. Anagnostopoulos, M. Faghri, *Lab Chip* **2012**, *12*, 2909.
[26] C.-M. Cheng, A. W. Martinez, J. Gong, C. R. Mace, S. T. Phillips, E. Carrilho, K. A. Mirica, G. M. Whitesides, *Angew. Chem. Int. Ed.* **2010**, *49*, 4771.
[27] W. Dungchai, O. Chailapakul, C. S. Henry, *Anal. Chem.* **2009**, *81*, 5821.
[28] J. Yu, L. Ge, J. Huang, S. Wang, S. Ge, *Lab Chip* **2011**, *11*, 1286.
[29] J. L. Delaney, C. F. Hogan, J. Tian, W. Shen, *Anal. Chem.* **2011**, *83*, 1300.
[30] J. Yan, L. Ge, X. Song, M. Yan, S. Ge, J. Yu, *Chem. Eur. J.* **2012**, *18*, 4938.
[31] C. H. Lee, L. Tian, S. Singamaneni, *ACS Appl. Mater. Interfaces* **2010**, *2*, 3429.
[32] L. Ge, J. Yan, X. Song, M. Yan, S. Ge, J. Yu, *Biomaterials* **2012**, *33*, 1024.
[33] D. Zang, L. Ge, M. Yan, X. Song, J. Yu, *Chem. Commun.* **2012**, *48*, 4683.
[34] L. Ge, S. Wang, X. Song, S. Ge, J. Yu, *Lab Chip* **2012**, *12*, 3150.
[35] S. Wang, L. Ge, X. Song, J. Yu, S. Ge, J. Huang, F. Zeng, *Biosens. Bioelectron.* **2012**, *31*, 212.
[36] W. Dungchai, O. Chailapakul, C. S. Henry, *Anal. Chim. Acta* **2010**, *674*, 227.
[37] E. Fu, T. Liang, J. Houghtaling, S. Ramachandran, S. A. Ramsey, B. Lutz, P. Yager, *Anal. Chem.* **2011**, *83*, 7941.
[38] J. Liang, Y. Wang, B. Liu, *RSC Adv.* **2012**, *2*, 3878.
[39] M. M. Ali, S. D. Aguirre, Y. Xu, C. D. M. Filipe, R. Pelton, Y. Li, *Chem. Commun.* **2009**, *45*, 6640.
[40] J. Liu, D. Mazumdar, Y. Lu, *Angew. Chem. Int. Ed.* **2006**, *45*, 7955.
[41] W. Zhao, M. M. Ali, S. D. Aguirre, M. A. Brook, Y. Li, *Anal. Chem.* **2008**, *80*, 8431.
[42] K. Haupt, *Anal. Chem.* **2003**, *75*, 376A.
[43] K. Haupt, K. Mosbach, *Chem. Rev.* **2000**, *100*, 2495.
[44] X.-M. Li, X.-Y. Yang, S.-S. Zhang, *TrAC, Trends Anal. Chem.* **2008**, *27*, 543.
[45] A. Apilux, W. Dungchai, W. Siangproh, N. Praphairaksit, C. S. Henry, O. Chailapakul, *Anal. Chem.* **2010**, *82*, 1727.
[46] Z. Nie, C. A. Nijhuis, J. Gong, X. Chen, A. Kumachev, A. W. Martinez, M. Narovlyansky, G. M. Whitesides, *Lab Chip* **2010**, *10*, 477.
[47] Z. Nie, F. Deiss, X. Liu, O. Akbulut, G. M. Whitesides, *Lab Chip* **2010**, *10*, 3163.
[48] P. Wang, L. Ge, M. Yan, X. Song, S. Ge, J. Yu, *Biosens. Bioelectron.* **2012**, *32*, 238.
[49] R. Pelton, *TrAC, Trends Anal. Chem.* **2009**, *28*, 925.
[50] C. Holden, *Science* **2003**, *300*, 1866.
[51] M.-F. Ritz, P. Schmidt, A. Mendelowitsch, *Neurochem. Res.* **2002**, *27*, 1677.
[52] M. Zayats, R. Baron, I. Popov, I. Willner, *Nano Lett.* **2004**, *5*, 21.
[53] K. Liu, W.-Z. Wei, J.-X. Zeng, X.-Y. Liu, Y.-P. Gao, *Anal. Bioanal. Chem.* **2006**, *385*, 724.
[54] J. Lu, S. Ge, L. Ge, M. Yan, J. Yu, *Electrochim. Acta* **2012**, *80*, 334.
[55] X. Gong, X. Yi, K. Xiao, S. Li, R. Kodzius, J. Qin, W. Wen, *Lab Chip* **2010**, *10*, 2622.
[56] B. D. Busbee, S. O. Obare, C. J. Murphy, *Adv. Mater.* **2003**, *15*, 414.